JOURNAL OF MATERIALS SCIENCE 26 (1991) 726–736

Microstructure and properties of SiC whisker reinforced ceramic composites

M. YANG*, R. STEVENS
School of Materials, The University of Leeds, Leeds, LS2 9JT, UK

Microstructures of SiC whisker reinforced alumina and tetragonal zirconia polycrystals (TZP) were investigated using analytical electron microscopy. In the Al_2O_3–SiC system, amorphous phases between the whisker and matrix were observed; these amorphous phases were virtually eliminated when the whiskers were leached with HF acid before being incorporated into the matrix. In the TZP/SiC system, reaction between the whisker and matrix had taken place during fabrication and resulted in the formation of a glassy phase. This reaction appeared to be associated with the presence of SiO_2 impurity present in the TZP matrix.

Mechanical properties of the composites were measured both at ambient and elevated temperatures and fracture surfaces were examined. The results indicated that fracture of the composites was sensitively influenced by the whisker–matrix interface. The presence of amorphous interfacial phases was detrimental to the properties of the composites and caused a reduction in fracture energy. High temperature tests showed that the TZP composite had a structural transition with extensive cracking occurring at 1000 °C, whilst the alumina composites retained their properties up to 1200 °C, whereupon they deteriorated rapidly.

1. Introduction

Recently there has been considerable interest in the development of SiC whisker reinforced ceramic composites. Extensive research has been carried out and significant progress has been achieved in the fields of processing technology and the understanding of the mechanical behaviour of the composite [1–6]. It has been shown that the fracture toughness of brittle ceramics can be effectively improved via the incorporation of strong and stiff SiC whiskers by means of crack deflection and fibre pull-out. These toughening mechanisms do not diminish as the temperature increases and thus have an advantage over transformation toughening. In addition, the whisker reinforced ceramic composites possess some important properties such as hardness and wear resistance as well as physical and chemical stability which make them very attractive for wear applications and for use in a corrosive environment [7].

The whisker reinforced ceramic composite is nevertheless a new type of material. A detailed knowledge of the fibre–matrix interface is required as well as a thorough understanding of the fracture process of the composite under specified test conditions in order to optimize the properties of the material. The object of this study is to assess the microstructure of alumina and tetragonal zirconia polycrystals (TZP) composites reinforced with SiC whiskers using analytical electron microscopy, and to analyse the mechanical behaviour and properties of the composite. Finally the combined data will be used to interpret the role of the interface in connection with the mechanical properties of the composite.

2. Experimental procedure

The materials used in this study were alumina and TZP composites reinforced with up to 30 vol % SiC whiskers. The whiskers were supplied by the Nikkei Carbon Co. Ltd, having a diameter less than 1 μm and length up to 100 μm. The whiskers were leached with 5 vol % HF acid for 10 h and washed five times with distilled water to remove the oxide rich layer present on the surface of the as-received whiskers. Both the as-received and leached whiskers were incorporated into the matrices in order to elucidate the effect of interfacial phases on the properties of the composites. The alumina and TZP composites were hot pressed at pressure of 27 MPa and temperatures of 1800 and 1650 °C, respectively. Details related to the fabrication of the composites have been reported in a previous article [8].

The Young's modulus of the composite was measured by the sound resonance technique. Flexural strength was determined in a three-point bending test using an Instron machine. The test was conducted at a cross-head speed of 0.1 mm min^{-1}. The nominal dimensions of the specimen were 25 × 4 × 3 mm^3.

Chevron-notched specimens were employed for the determination of fracture energy. Specimens with the same dimensions as those used for the strength

* *Present address*: School of Materials Science, University of Bath, Bath, BA2 7AY, UK

0022–2461/91 $03.00 + .12

test were notched with a 0.236 mm thick diamond blade. The test was performed in three-point bending on the Instron machine at a cross-head speed of 0.05 mm min^{-1}. The fracture energy was calculated from the area covered underneath the load–deflection curve divided by twice the fracture surface area of the specimen.

Fracture surfaces of the composites were examined using a Camscan 300 scanning electron microscope (SEM). Specimens for transmission electron microscopic (TEM) studies were prepared by cutting thin sections from the hot-pressed disc. The thin section was mechanically polished to a thickness of less than 40 μm, then sandwiched between a pair of copper "hole" grids. Finally it was ion milled using the Gatan ion beam thinner at a voltage of 4 kV and an incidence beam angle of 15° until the specimen was perforated, and further treated at the beam incidence angle of 10° for another 20 min to yield a larger area, transparent to the electron beam.

TEM examination was performed on a Jeol2000EX with an operating voltage of 200 keV using a side entry double-tilt specimen holder. A cold trap filled with liquid nitrogen was attached to the holder to minimize contamination of the specimen during analysis. A windowless energy dispersive spectrometer (EDS) was employed, with a spatial resolution better than 20 nm and capable of detecting light elements such as carbon and oxygen.

3. Results and discussion

3.1. Transmission electron microscopy

Fig. 1 shows a typical structure of the alumina composite containing 20 vol % SiC whiskers. The specimen was prepared by cutting a thin section from the hot-pressed disc normal to the pressing axis. The whiskers were seen along their axis because of their preferential alignment in this plane. The serrated surfaces of the whiskers appeared to have a good bond with the matrix. Extensive contrast bands across the matrix were typical of the specimen. This suggested that there were residual thermal stresses in the composite due to the difference in the thermal expansion coefficient between the whisker and matrix. When viewed parallel to the hot-pressing axis, only the cross-section of the whiskers was seen, with faceted features as in Fig. 2. It was apparent that the majority of the whiskers were located at matrix grain boundaries. This indicated that the whiskers had the required pinning effect necessary to impede grain growth during hot pressing.

Interfacial regions between the whisker and the matrix were examined at high magnification. Fig. 3 shows a bright field image of the Al_2O_3 composite with the as-received whiskers. The whisker was identified as ß-SiC with high density of stacking faults on the (111) planes. These planar faults caused severe streaking of the diffraction spots in the [1 1 1] direction. The contrast at the contacting interface in the marked area further confirmed the presence of residual thermal stresses. An amorphous film was obviously present at the periphery of the whisker with

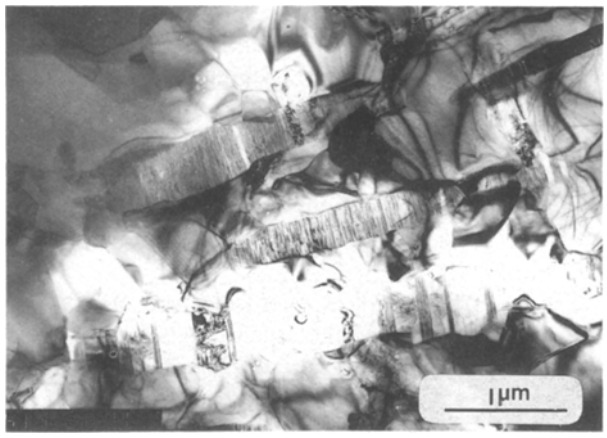

Figure 1 TEM micrograph of the alumina composite showing the preferential alignment of the whiskers in the hot-pressing plane and good bonding between the whiskers and matrix. Note the contrast bands from the whisker into the matrix, indicating high elastic strains.

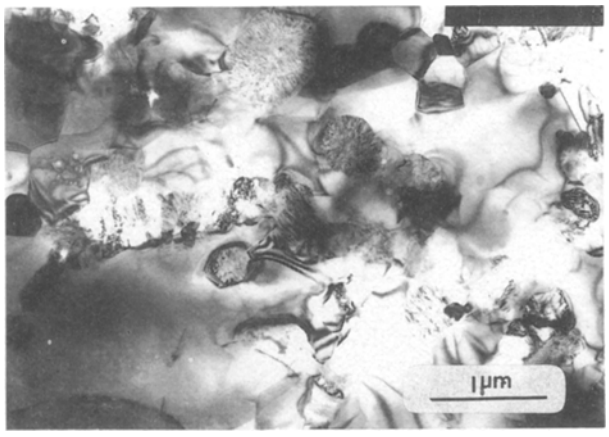

Figure 2 TEM micrograph of the alumina composite showing the faceted transverse section of the whiskers, the majority of which are located at matrix grain boundaries.

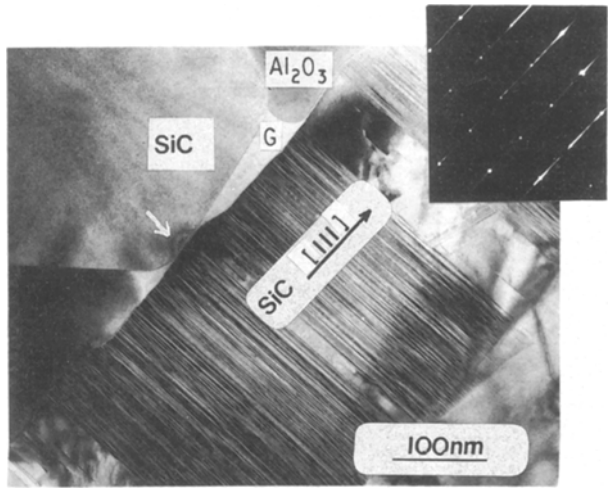

Figure 3 TEM micrograph of the alumina composite with the as-received whisker showing an amorphous phase at the whisker–matrix interface with sizeable pockets of glass at triple points.

sizable pockets of glass at triple points. In comparison, when the whiskers were leached before being incorporated into the matrix, the whisker–matrix interface was virtually free from any amorphous phase, as

shown in Fig. 4, in which the whisker showed microtwins less than 10 nm in thickness, and the (1 1 1) fringes of the alumina lattice joined the whisker at their interface, where no glassy phase was possibly present. It can thus be assumed that the Al_2O_3–SiC system was stable at the fabrication conditions, and the interfacial amorphous phase mainly stemmed from the silica-rich layer present on the as-received SiC whiskers.

Fig. 5 shows a typical microstructure of the TZP composite containing the leached whiskers. Lattice images taken from the marked region in Fig. 5 are illustrated in Fig. 6. It is apparent that the (1 1 1) fringes of the SiC lattice with a spacing of 0.25 nm joined the (1 1 1) fringes of the tetragonal zirconia lattice with a spacing of 0.296 nm at the interface, where little or no amorphous phase was observed. The micrograph shown in Fig. 7, however, revealed a large quantity of glass present at the whisker–matrix interface, as indicated by the diffuse electron diffraction pattern. The EDS pattern showed that the glass had a composition based on zirconium, silicon, oxygen and carbon. The whisker in Fig. 7b had an eroded appearance. Further examples are shown in Fig. 8, in which the whisker and matrix were separated by a thin layer of amorphous phase.

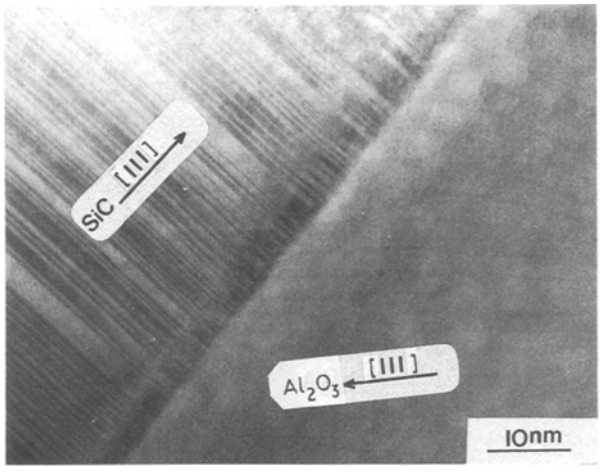

Figure 4 Lattice imaging of the alumina composite with the leached whisker showing the (111) fringes of the alumina lattice joined directly to the whisker at their interface.

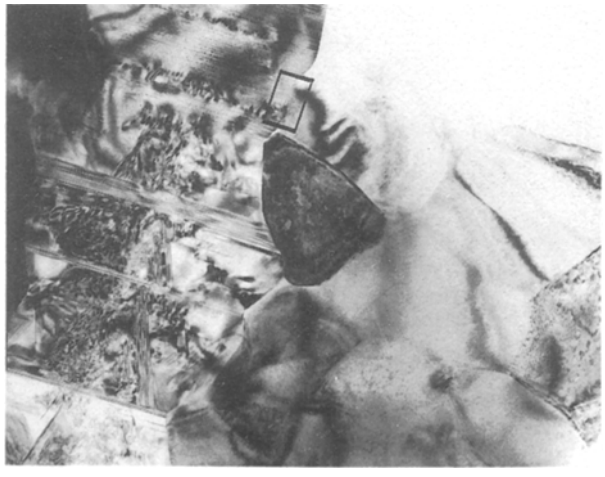

Figure 5 Typical interfacial structure of the TZP composite with the leached whisker.

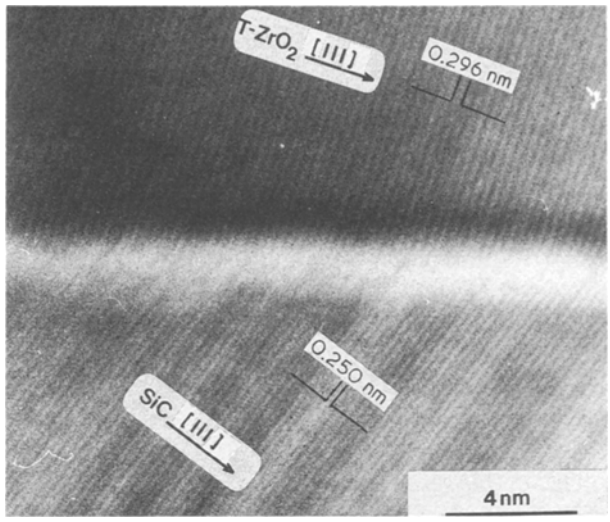

Figure 6 Lattice images of the marked region in Fig. 5 indicating little or no amorphous phase between the whisker and TZP matrix.

A reaction between SiC and ZrO_2 has been reported previously [9], and is believed to proceed according to the following equation

$$SiC + ZrO_2 \Rightarrow ZrC + SiO_{(g)} + CO_{(g)}$$

Gauckler and Petzow [9] found that the addition of Al_2O_3–SiO_2, which formed a transient liquid phase and facilitated quick densification, could effectively depress the gas producing reaction. They argued that the existence of Al_2O_3 and SiO_2 raised the oxygen activity and thus avoided the reaction. This explanation is apparently not convincing because any increase in the oxygen content would reduce the concentrations of SiO and CO and make the reaction proceed towards the right direction. This appears to be confirmed by the present experimental result.

3.2. Elastic behaviour

As mentioned previously, the SiC whiskers were preferentially aligned in the plane normal to the hot-pressing axis. The elastic behaviour of the composite in this plane was anticipated to be isotropic and was measured using the sound resonance technique. Three bars of each composition were tested and the experimental results are listed in Tables I and II.

The tabulated data indicate that the results obtained from the sound resonance technique were consistent. The elastic modulus of the alumina composite remained almost the same as that of the matrix. The deviation in each set of data appeared to widen when whisker content was increased. This deviation can be explained on the basis of the microstructural homogeneity of the composite, the degree of which is likely to decrease with increasing whisker loading, thereby causing a wider fluctuation of the property.

Taking account of the effect of porosity on the elastic modulus of the composites and applying

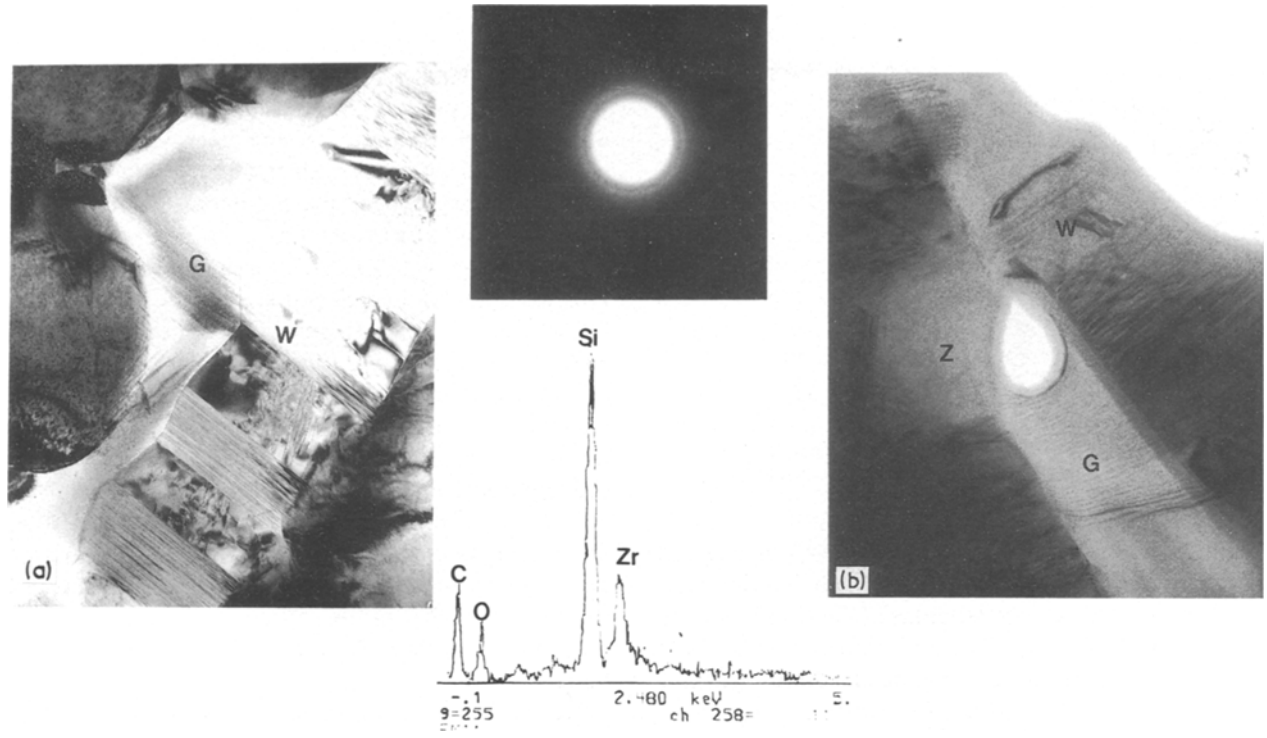

Figure 7 TEM micrographs of the TZP composite showing a large quantity of glass phase at the whisker–matrix interface. The EDS spectrum indicates that the composition of the glass is made of Si, Zr, C and O.

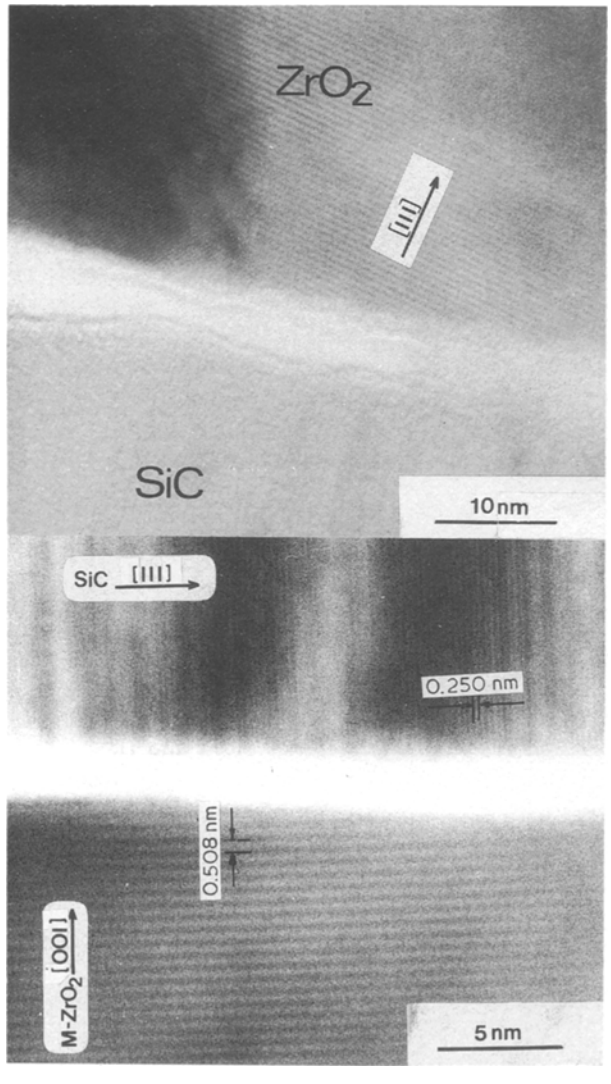

Figure 8 Lattice images of the TZP composite showing that the whisker and matrix are separated by an amorphous phase.

TABLE I Elastic modulus of the SiC–Al_2O_3 composites

SiCw content (vol %)	0	10	20	30
Average porosity (%)	0	0.5	1.0%	1.5%
Elastic modulus (GPa)	396.9	397.0	394.6	394.1
	397.0	397.6	394.9	397.4
	397.2	397.7	393.7	398.9
Average modulus (GPa)	397.0	397.4	394.4	396.8
Modulus at zero porosity (GPa)	397.0	401.0	403.4	408.2

TABLE II Elastic modulus of the SiCw–TZP composites

SiCw content (vol %)	0	10	20
Elastic modulus (GPa)	205	224	244

Mackenzie's equation [10], gives

$$E = E_0(1 - 1.9P - P^2)$$

where E is the measured modulus with porosity P, E_0 the elastic modulus of the fully dense material.

The elastic modulus of the composite at zero porosity can be extrapolated and the results are plotted in Fig. 9 together with the results calculated from Voigt and Reuss equations, assuming the modulus of the whiskers to be 440 GPa.

Theoretically, the Voigt and Reuss equations provide the upper and lower bounds of the elastic modulus of composites. It is reasonable that the extrapolated data fall between these two bounds. It may be necessary to point out that the choice of the elastic modulus of the SiC whiskers for the theoretical computation is far from obvious because there are a large

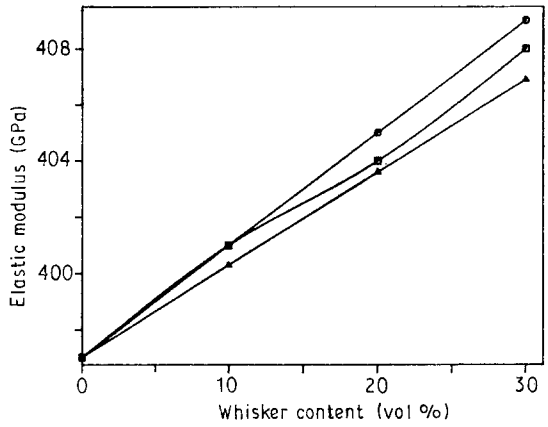

Figure 9 Correlation of the experimentally measured (□) elastic moduli of the alumina composite with theoretical predictions (○ Voigt, △ Reuss).

number of different values quoted for SiC whiskers in the literature. For instance, Yerkvonitch and Kirchner [11] reported the elastic modulus of the whiskers to be in the range of 89 to 890 GPa. Petrovic *et al.* [12] found that the modulus of the CVD ß-SiC whiskers varied between 360 and 870 GPa with an average of 560 GPa, therefore, the average determined from so wide a range can hardly be accurate.

Since the whiskers are randomly oriented in the matrix, the elastic behaviour of individual whiskers is presumed to be similar to that of grains in the polycrystalline SiC material, in which the orientation dependent contributions of individual grains balance each other and the experimental error is minimized. The average of the modulus of the polycrystalline SiC is thus believed to be representative of the whiskers in the composite. A value of 440 GPa, typical of the hot-pressed ß-SiC [13], has been shown to be applicable and can also be used to account for the discrepancy observed by other authors [3, 14].

3.3. Fracture energy

Fracture energy is a well defined property of materials, and represents that energy required to create a unit surface area. In practice, it has to be determined when the process of fracture is stable, such that the total energy expended by the external work is absorbed in the fracture process. Several techniques have been developed to estimate fracture energy. The results obtained typically vary with testing methods, the geometry of the specimen, and the microstructure of the material tested. For example, in the single-edge notched beam test, fracture is initiated from the pre-notched crack and crack propagation is so rapid that the specimen fails catastrophically. Hence, the fracture energy measured using this method only reflects the energy required at the moment of crack initiation, regardless of the crack interaction in the late stages. In the double cantilever or double torsion tests, crack propagation can be better controlled. However, the complexity of the specimen geometry and the testing procedure has limited their popularity. In comparison, the Chevron notched beam method has advantages, i.e. the simplicity of the specimen and the testing procedure, together with a controlled crack propagation.

Nevertheless, several factors were found to affect an accurate measurement using the Chevron-notched beam method. Firstly, Tattersall and Tappin [15] noticed that a stiff load cell was favoured because more elastic energy was likely to be stored in the soft load cell, which could cause destabilization of crack growth. Secondly, Simpson [16] found that the stability of crack growth increased with the decreasing notch depth ratio, and that the measured fracture energy became smaller until maximum stability was reached.

In view of the difficulties involved and the numerous factors affecting measurements of fracture energy, few conclusions can be drawn. Davidge [17] has suggested that it is best to regard fracture energy as an empirically determined parameter. With this in mind, the fracture energy of the composite was measured using the Chevron-notch method. The experimental variables considered here are the notch ratio ($h/b = 0.5$, see Fig. 10) and the cross-head speed (0.05 mm min^{-1}).

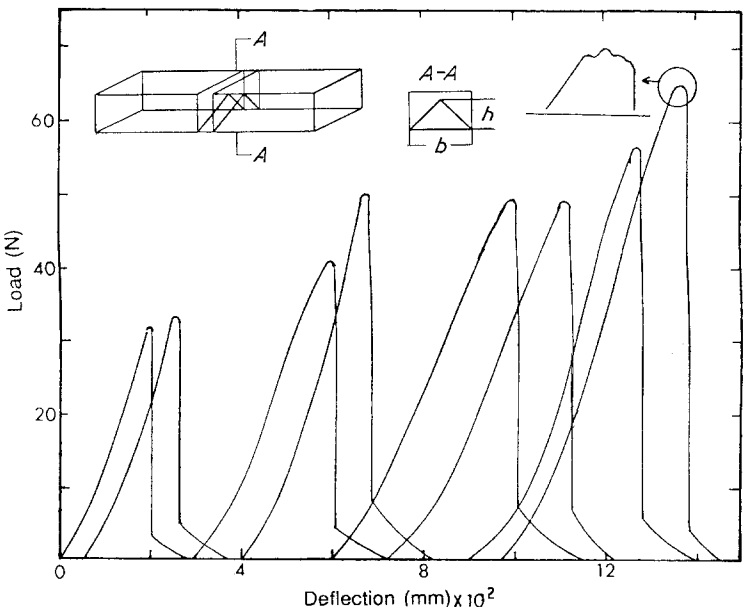

Figure 10 Normalized load–deflection curves of the alumina composite with leached whiskers

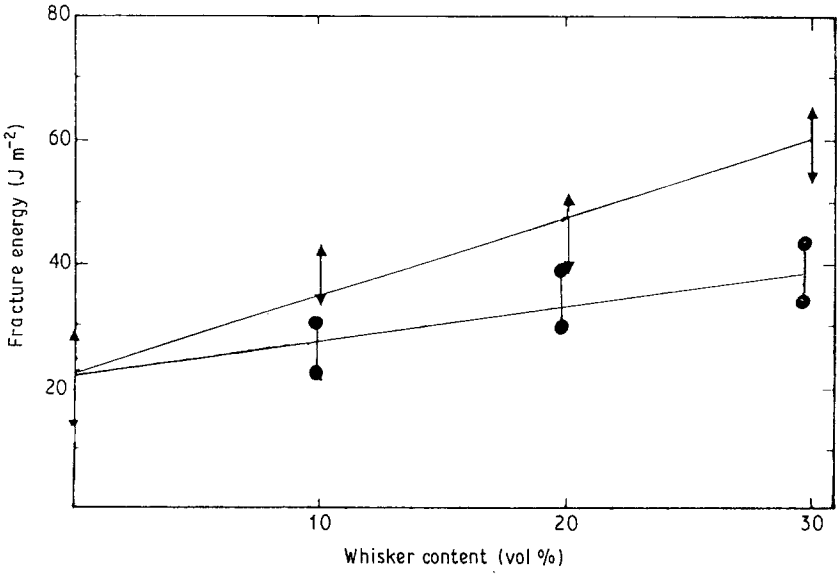

Figure 11 Comparison of the fracture energy of the composite with the as-received (●) and leached (▲) whiskers.

Fig. 10 represents typical load–deflection curves, in which the fracture surface area was normalized such that the failure load–deflection curves were comparable. At the moment of fracture, there was evidence of crack stick and slip, as indicated by the enlarged area in Fig. 10. After fracture, the load dropped drastically, but not completely, suggesting crack propagation to be semi-stable during the test.

The fracture energy of the composite is plotted in Fig. 11, and shows an increasing trend with whisker content. The hot-pressed alumina had an average value of 20 J m^{-2}, whereas the alumina composite with 30 vol % leached whisker had a value of fracture energy three times as high as that of the monolithic matrix. In contrast, a much lower increase in the fracture energy was observed for the composite with the as-received whiskers, as indicated by the bottom line in Fig. 11.

This difference can be explained by microstructural examination. Fig. 12 shows the fracture surface of the composite with the leached whiskers. It appeared to be rather uneven, indicating that the crack path had been deflected by the reinforcing whiskers. In comparison, the composite containing the as-received whiskers had a flat appearance, as shown in Fig. 13. This clearly suggested that the presence of the amorphous phase at the whisker–matrix interface had embrittled the composite, allowing the crack to proceed across the whiskers avoiding deflection and thereby causing a reduction in fracture energy.

From the above observation, it is believed that the increase in fracture energy by the whisker reinforcement is mainly due to the crack deflection mechanism. This mechanism assumes that the crack is initiated in the matrix and expands around the whiskers. As the crack changes its direction, its orientation relative to the applied stress will change and it will therefore require more energy to extend further. Further evidence for crack interaction is provided by TEM observations. Fig. 14 shows that a crack from the matrix extended towards a whisker interface. The crack was then diverted along the interface and turned back to the matrix. Fig. 15 illustrates the possibility of crack bridging and deflection by a whisker.

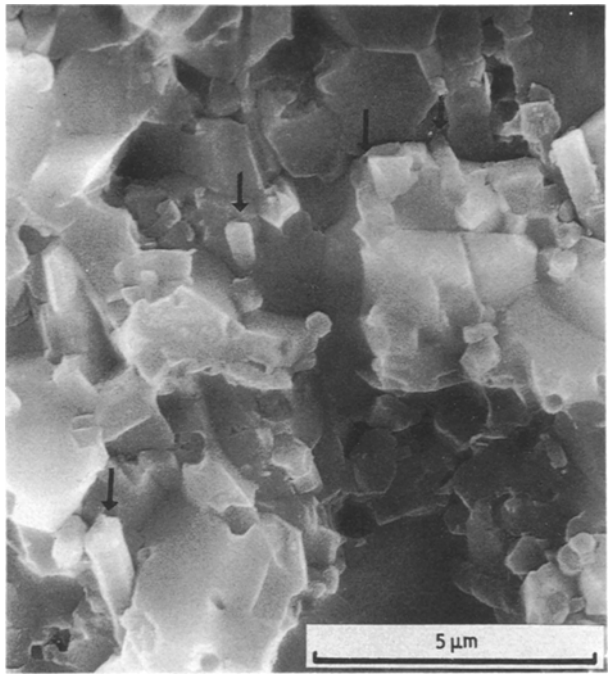

Figure 12 Fracture surface of the alumina composite with the leached whiskers.

Provided that the aspect ratio of the whiskers is greater than 20, the increment in fracture energy predicted from the Faber–Evans model [18] should be at least ten fold. This is considerably higher than the present experimental data, a discrepancy believed to be caused by the degree of crack deflection which is allowed to take place in the practical system. In the theoretical model, cracks are assumed to be diverted along the maximum length of the whiskers. In practice, this can hardly be realised due to the strong interfacial bonding between the whisker and matrix. This implies that only a small portion of the whiskers actually takes part in crack deflection. The results may, therefore, indicate that the aspect ratio of the whiskers can be reduced to a certain value but the toughening efficiency will not be diminished. This has practical significance since it is much easier to handle shorter whiskers during fabrication. Aggregation of

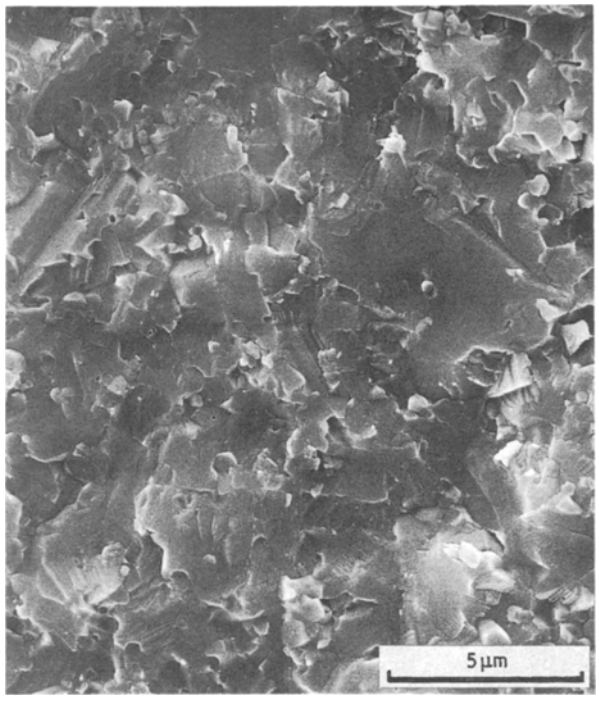

Figure 13 Fracture surface of the alumina composite with the as-received whiskers.

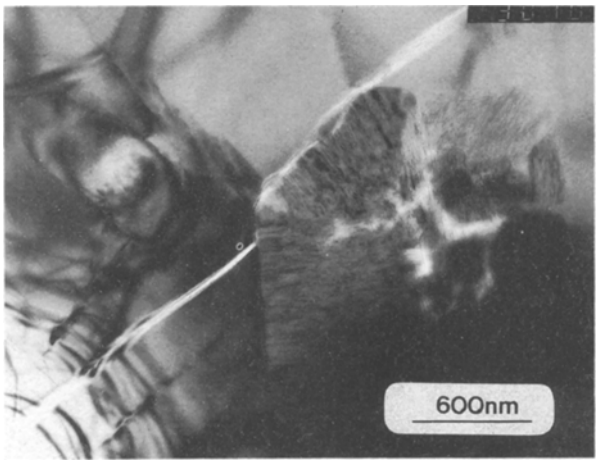

Figure 14 TEM micrograph of the alumina composite showing a crack being deflected along the whisker–matrix interface.

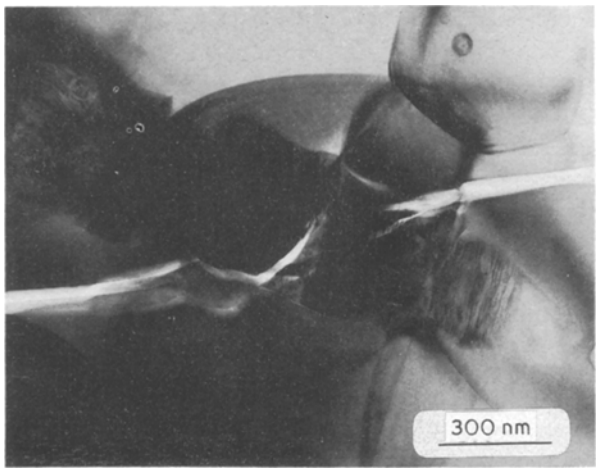

Figure 15 TEM micrograph of the alumina composite showing a crack being partially bridged by a whisker. Deflection of the crack along the interface is apparent.

shorter whiskers is less likely to occur during mixing, and processing temperature can be reduced substantially, as demonstrated by the hot-pressing kinetic studies.

3.4. Flexural strength

The strength of the alumina composites is plotted as a function of the whisker content in Fig. 16. The hot-pressed alumina had a flexural strength ranging from 527 to 570 MPa with an average value of 545 MPa. The strength of the composite increased slightly with increasing whisker content.

Typical load–deflection curves of the alumina composites are reproduced in Fig. 17. In general, the load–deflection curve showed an initial non-linear

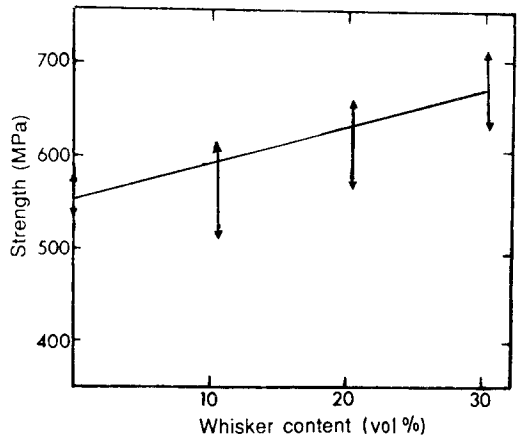

Figure 16 Plot of strength of the alumina composite against leached whisker content.

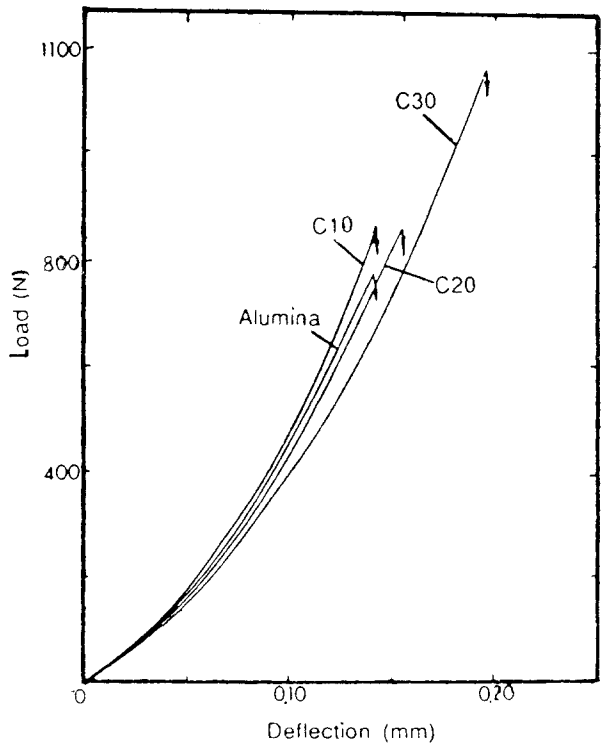

Figure 17 Typical load deflection curves of the alumina composite with 0 to 30 vol % SiC whisker. (C30 means the composite with 30 vol % whiskers)

region, followed by a linear region, until the specimen failed catastrophically. The initial non-linearity could be caused by the "bedding in" of the test machine due to its "softness". It is difficult to ascertain from the curves that there is non-linear deflection due to crack arresting by the whiskers in the process of fracture. It is believed that the fracture of the composite was controlled by the pre-existing defects, rather than by a defect produced by the deformation process.

It is at times possible to identify the origin of failure on the fracture surfaces of the composite. Fig. 18 shows the fracture surface of the composite having 20 vol % whiskers, failure of which was apparently initiated from a flaw near the tensile surface. The flaw was surrounded by a symmetrical fracture feature. High magnification examination, Fig. 19, revealed a large grain sitting at the flaw site. Circumferential cracks around the grain were noted. Taking the value for the fracture energy, $\gamma = 49\ \mathrm{J\,m^{-2}}$, the flaw size (equal to the radius of the large grain), $C = 20\ \mu\mathrm{m}$, $E = 400$ GPa, the strength of the composite is calculated to be 558 MPa, which is in good agreement with the measured strength of the material.

The effect of porosity on the strength of the alumina composite with 20 vol % SiC whiskers is illustrated in Fig. 20. As anticipated, the strength decreases with the increasing porosity. Using the least squares method,

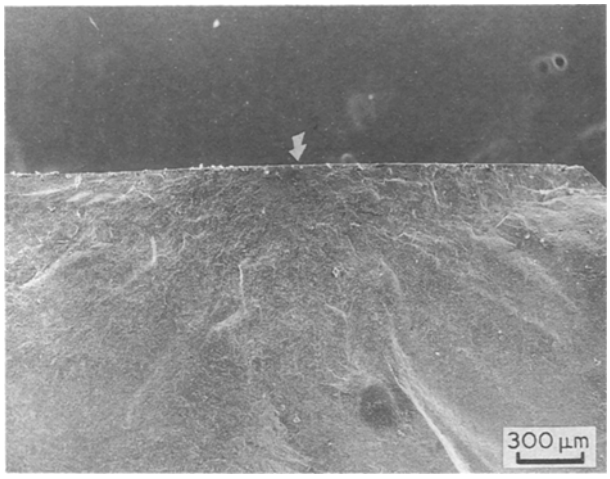

Figure 18 SEM micrograph of the alumina composite showing the origin of failure on the fracture surface.

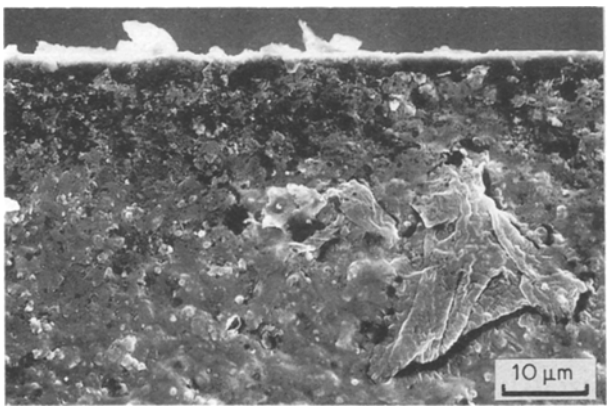

Figure 19 High magnification SEM micrograph showing a large grain sitting at the flaw site.

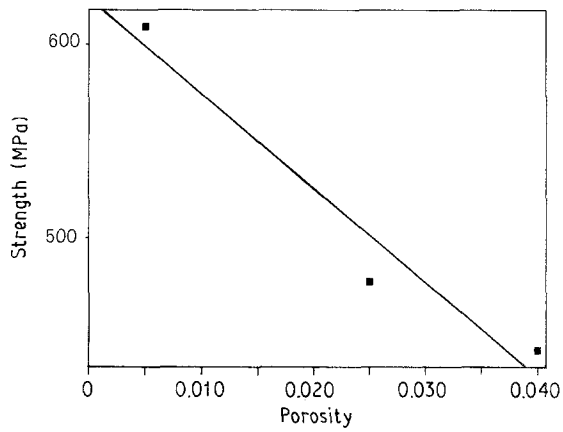

Figure 20 Effect of porosity on the strength of the alumina composite with 20 vol % leached whiskers. (slope = $-3.8520 + 00$, intercept = $2.7960 + 00$.

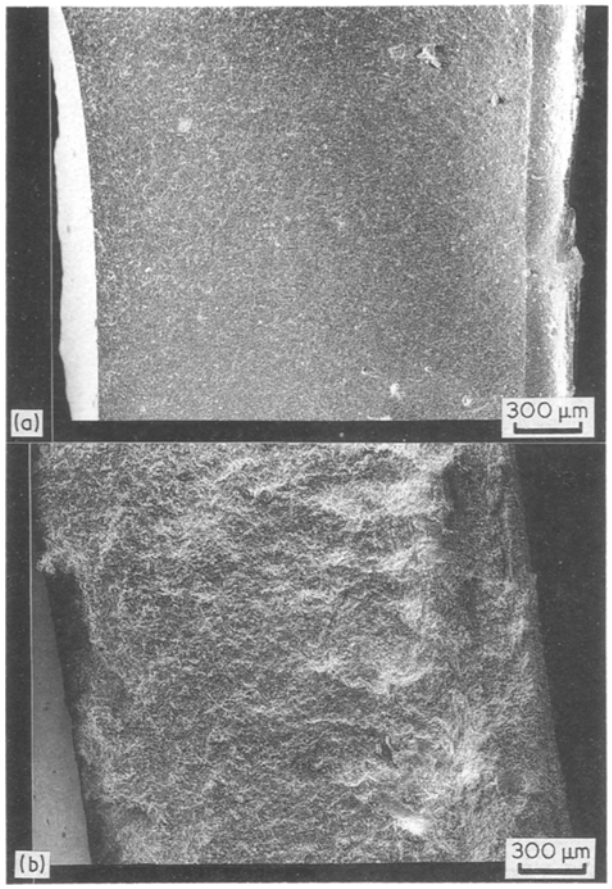

Figure 21 Fracture surfaces of (a) slip cast alumina (b) slip cast composite with 10 vol % whiskers.

an exponential relationship between the strength and porosity can be fitted to the data point as follows

$$\sigma = 616 \exp(-8.87p)$$

A similar relationship between the strength and porosity has been proposed for hot-pressed Al_2O_3 materials with a grain size of 2.2 μm and grain boundary porosity in the range of 0.2 to 6.55 [19]. The exponential constant determined for the Al_2O_3 was 9.4, which was slightly higher than that for the composite. This may imply that the strength of the composite decreases less with porosity than that of the unreinforced material and that relative load transfer from the matrix to the

fibre is more efficient so that the relative reinforcing efficiency is increased. This explanation is reinforced by an example shown in Fig. 21, in which the slip cast alumina compact is fragile, whereas the composite with 10 vol % whiskers having a similar density is much stronger. Fig. 21a shows the fracture surface of the slip cast alumina which appears to be smooth. In contrast, the fracture surface of the composite is rather rough, Fig. 21b, suggesting that extensive crack whisker interactions have taken place.

The strength of the hot-pressed TZP composites is shown in Fig. 22. The TZP material has an average strength of 1067 MPa. In comparison, the strength of the composites diminished when the whisker content was increased. For example, 876 MPa was obtained as the flexural strength for the composite with 20 vol % whiskers.

The decreasing strength of the TZP composites with whisker content has also been observed by Claussen *et al.* [3]. Two explanations seem to be possible for this behaviour. The first is the grain size of the hot-pressed TZP material is approximately 0.3 μm, which is substantially smaller than that of the TZP matrix in the composite, as can be seen in Figs 23 and 24. The effect of grain size on the flexural strength has been widely interpreted using the Hall–Petch type relationship [20]

$$\sigma = f(G^{-1/2})$$

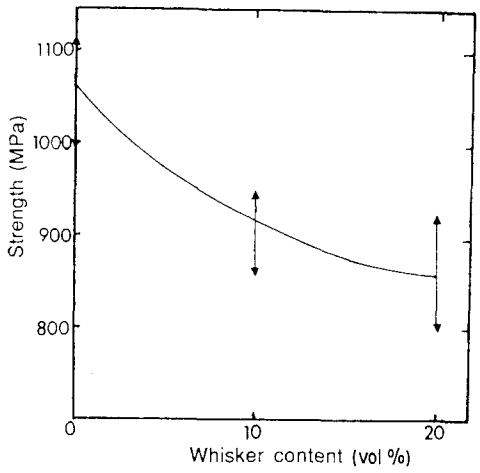

Figure 22 Plot of strength of the TZP composite against leached whisker content.

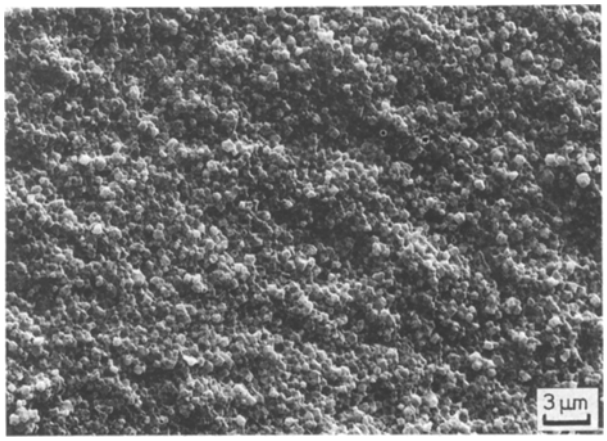

Figure 23 Fracture surface of the hot-pressed TZP material.

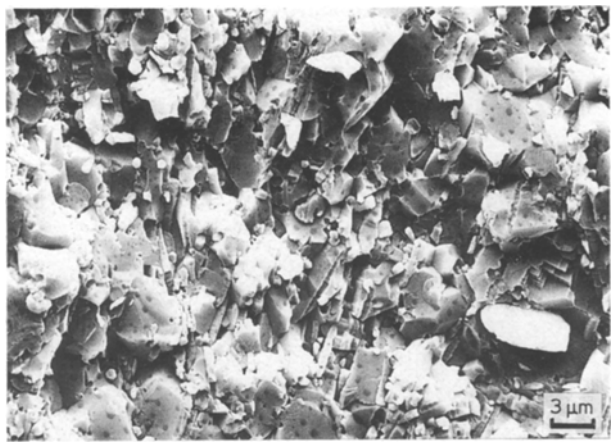

Figure 24 Fracture surface of the TZP composite with 20 vol % leached whiskers.

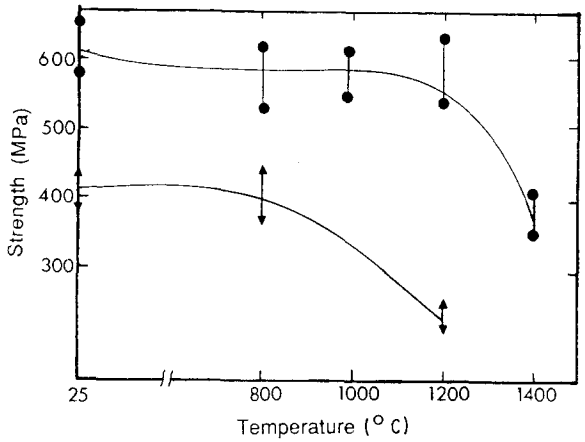

Figure 25 Plot of strength of the alumina composite against temperature (● C20 composite, ▲ hot-pressed alumina).

where σ is the flexural strength and G the grain size. Secondly, it is expected that the residual thermal stresses can be developed because of the difference in thermal expansion coefficients between the whiskers and the matrix. The approximate stress developed may be estimated from the following equation [21]

$$\sigma_t = \frac{E_f V_f \Delta\alpha \Delta T}{1 + V_f(E_f/E_m - 1)}$$

Taking the elastic modulus of the matrix (E_m) and the whiskers (E_f) as 200 and 400 GPa, respectively, $\Delta T = 1200$, $\alpha_{SiC} = 4.5 \times 10^{-6} K^{-1}$, $\alpha_{TZP} = 9.5 \times 10^{-6} K^{-1}$, a stress value of 483 MPa can be obtained for the composite with 20 vol % whiskers. The tensile stressed matrix is to be the favoured site for crack nucleation. Consequently, the reinforcing effect of the whiskers can be overridden by such a combination of these two factors, the composite being weaker than the monolithic matrix.

3.5. High temperature strength

The strength of the alumina composite with the 20 vol % leached whiskers is plotted in Fig. 25 as a

function of temperature. The strength of the hot-pressed alumina with a grain size of 3 μm is also plotted in Fig. 25 for comparison [22]. It is evident that the properties of the hot-pressed alumina decreased dramatically above 800 °C, whereas the composite retained its strength up to 1200 °C, beyond which it deteriorated substantially.

Failure of polycrystalline alumina under stress at high temperature is known to be a consequence of creep deformation. The formation of grain boundary voids and cavities induced by stress and strain due to the unaccommodated grain boundary sliding leads to tertiary creep, which occurs readily at high temperature. The low creep resistance has been generally attributed to the occurrence of the diffusional creep mechanism [23]. A recent study [24] has shown that the alumina composite reinforced with SiC whiskers has a superior deformation resistance. A stress exponent of 5.2 was reported for the composite with 15 vol % whiskers compared to 1.6 for that of fine grain alumina deformed at 1500 °C.

The present study indicated that the effect of creep deformation on the high temperature failure of the composite was not significant at or below 1200 °C. At 1400 °C, failure of the composite was associated with grain boundary cavitation and crack coalescence, as a result of creep deformation. It was noted that the fracture surfaces of the composite were mainly transgranular below 1200 °C, Fig. 26, and intergranular along with the occurrence of whisker pull-out at 1400 °C, Fig. 27. Below 1200 °C, grain boundary sliding was hindered by the whiskers lying across the grain boundary, such that the formation of grain boundary cavities was avoided, and the failure of the composite was determined by pre-existing flaws. At 1400 °C, however, the interface between the whiskers and the matrix was so weakened that grain boundary sliding took place and the failure of the composite was then determined by creep deformation.

TEM examinations revealed that extensive dislocations occurred in the composites tested above 1200 °C. Fig. 28 shows an array of dislocations initiated from the whisker and extending into the matrix. Fig. 29 demonstrates the presence of a subgrain boundary of dislocations pinned at the whisker matrix interface. Such a dislocation network is typical of a "recovered

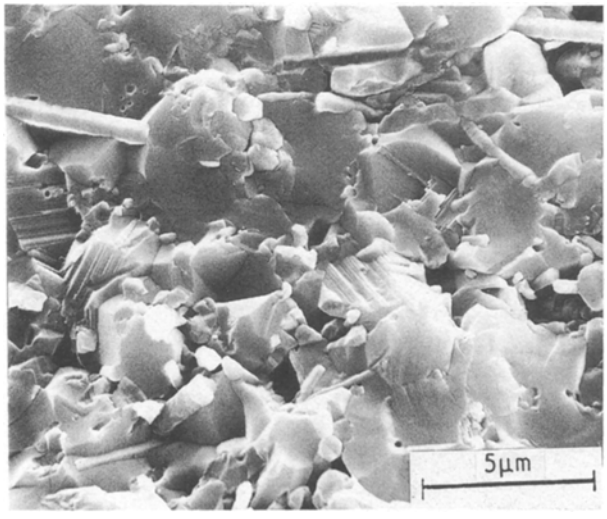

Fig. 26 Fracture surface of the alumina composite tested at 1200 °C.

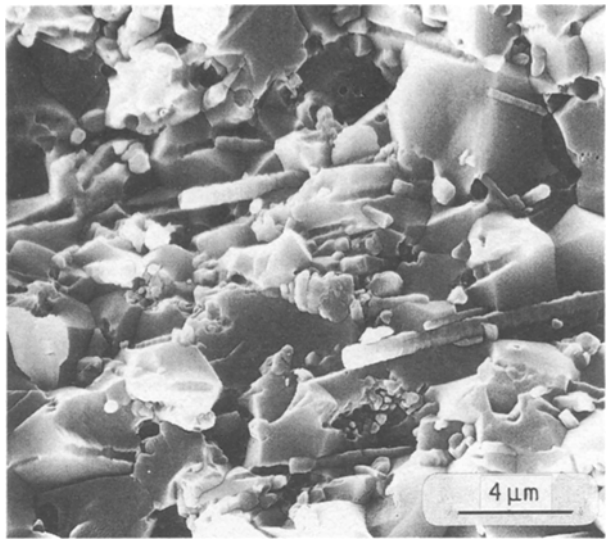

Figure 27 Fracture surface of the alumina composite tested at 1400 °C.

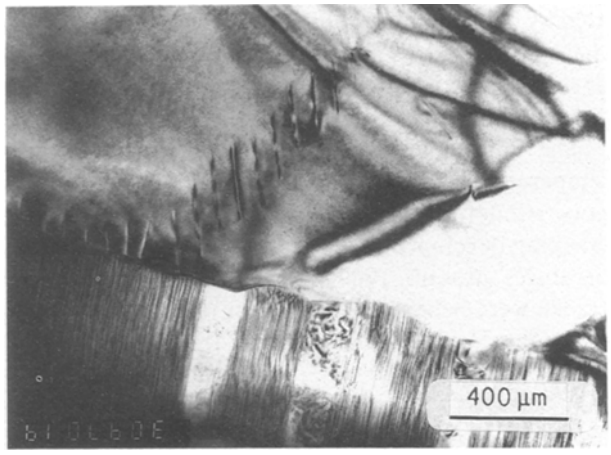

Figure 28 TEM micrograph of the alumina composite tested at 1200 °C showing an array of dislocation initiated at the matrix–whisker interface.

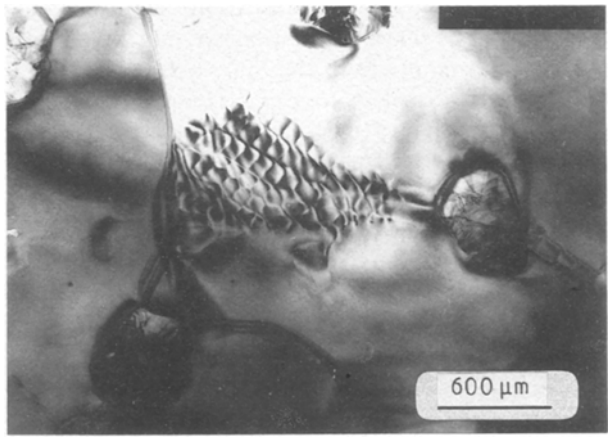

Figure 29 TEM micrograph of the alumina composite tested at 1200 °C showing a dislocation network nucleated at the whisker–matrix interface and pinned at the matrix grain boundary.

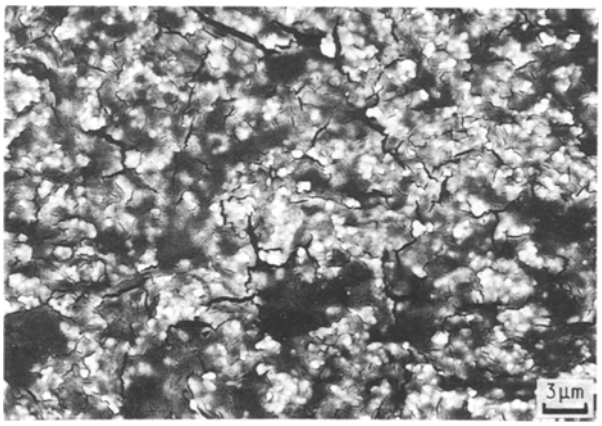

Figure 30 SEM micrograph of the TZP composite heat treated at 1000 °C revealed the occurrence of extensive cracking throughout the composite.

structure" where extensive dislocation arrays generated by deformation would form networks minimizing their strain energy. Such structures form on removal of stress by cross slip or climb which is possible at the elevated temperatures employed during testing.

The TZP composite was also tested at elevated temperature. Unfortunately, the composite had very poor strength because of the occurrence of extensive cracking developed throughout the composite at temperatures around 1000 °C, as seen in Fig. 30. The cracks were believed to form as a result of relaxation of the localized residual thermal stresses.

4. Conclusions

(1) The microstructure of the alumina and TZP composites reinforced with SiC whiskers were characterized. It has been observed that the Al_2O_3–SiC system was stable at the fabrication conditions, and the amorphous phase at the whisker–matrix interface was derived mainly from the SiO_2-rich layer present on the surface of the as-received whiskers. Reaction between SiC and ZrO_2 occurred at 1650 °C. This reaction appeared to be related to the presence of the SiO_2 impurity present in the TZP matrix.

(2) The presence of the amorphous phase at the interface was found to be detrimental to the properties of the composites and caused a reduction in fracture energy.

(3) The experimental elastic modulus of the composite can be correlated with predictions from the rule of mixtures if the modulus of the whiskers is assumed to be equivalent to that of polycrystalline SiC.

(4) The strength of the alumina composite showed an increasing trend with whisker content. In contrast, the strength of the TZP composite diminished as the whisker content increased. This has been explained in terms of grain size and residual stress present in the composites.

(5) High temperature annealing at 1000 °C showed that the TZP composite had undergone a breakdown in the structure with the occurrence of extensive cracking throughout the composite. The alumina composite retained its flexural strength up to 1200 °C, above which it deteriorated rapidly.

References

1. G. C. WEI and P. F. BECHER, *Amer. Ceram. Soc. Bull.* **64** (1985) 298.
2. P. F. BECHER and G. C. WEI, *J. Amer. Ceram. Soc.* **67** (1984) C267.
3. N. CLAUSSEN, W. L. WEISSKOPFE and M. RUHLE, *ibid.* **69** (1986) 288.
4. P. F. BECHER and T. N. TIEGS, *ibid.* **70** (1987) 651.
5. P. D. SHALEK, J. J. PETROVIC, G. F. HURLEY and F. D. GAC, *Amer. Ceram. Soc. Bull.* **65** (1986) 351.
6. M. YANG and R. STEVENS, in Proceedings of Science of Ceramics 14, Canterbury, 1987 (Elsevier, Amsterdam, 1987) p. 879
7. M. YANG, PhD Thesis, The University of Leeds (1988).
8. M. YANG and R. STEVENS, *J. Mater. Sci.* **25** (1990) 4658.
9. G. SCHNEIDER, L. J. GAUKLER and G. PETZOW in "Energy and Ceramics", edited by P. Vincenzini (Elsevier, Amsterdam, 1980) p. 399.
10. J. K. MACKENZIE, *Proc. Phys. Soc.* **B63** (1950) 2.
11. L. A. YERKVITCH and H. F. KIRCHNER, WADD-TR-61-252 (1962).
12. J. J. PETROVIC and J. V. MILEWSKI, *J. Mater. Sci.* **20** (1985) 1167.
13. J. A. COPPOLA and R. C. BRADT, *J. Amer. Ceram. Soc.* **55** (1972) 455.
14. K. P. GADKREE and K. CHYUNG, *Amer. Ceram. Soc. Bull.* **65** (1986) 370.
15. H. G. TATTERSALL and G. TAPPIN, *J. Mater. Sci.* **1** (1966) 296.
16. L. A. SIMPSON, *J. Amer. Ceram. Soc.* **57** (1972) 7.
17. R. W. DAVIDGE, in "Fracture Mechanics of Ceramics", Vol. 2, edited by R. C. Bradt, D. P. H. Hasselman and F. F. Lange, (Plenum, New York, 1973) p. 447.
18. K. T. FABER and A. G. EVANS, *Acta Metall.* **4** (1983) 565.
19. R. W. RICE, "Microstructure dependence of mechanical behaviour of ceramics in Treatise on Materials Science and Technology", Vol. 11, edited by R. K. MacCrone (Academic, London, 1977).
20. N. J. PETCH, *Phil. Mag.* **1** (1956) 866.
21. D. C. PHILLIPS, "Fibre reinforced ceramics in Handbook of Composites", edited by A. Kelly and S. T. Mileiki (North Holland, Amsterdam, 1983).
22. W. B. CRANDALL, D. H. CHUNG and T. J. GRAY in "Mechanical Properties of Engineering Ceramics", edited by W. W. Kriegel and H. Palmer, III (Wiley, New York, 1961) p. 349.
23. W. R. CANNON and T. W. LANGDON, *J. Mater. Sci.* **18** (1983) 1.
24. A. H. CHOSHI and J. R. PORTER, *J. Amer. Ceram. Soc.* **68** (1985) C144.

Received 18 December 1989
and accepted 9 January 1990